June 2016 VOL. 51, NO. 3

CLAY MINERALS

Journal of Fine Particle Science

GeoScienceWorld

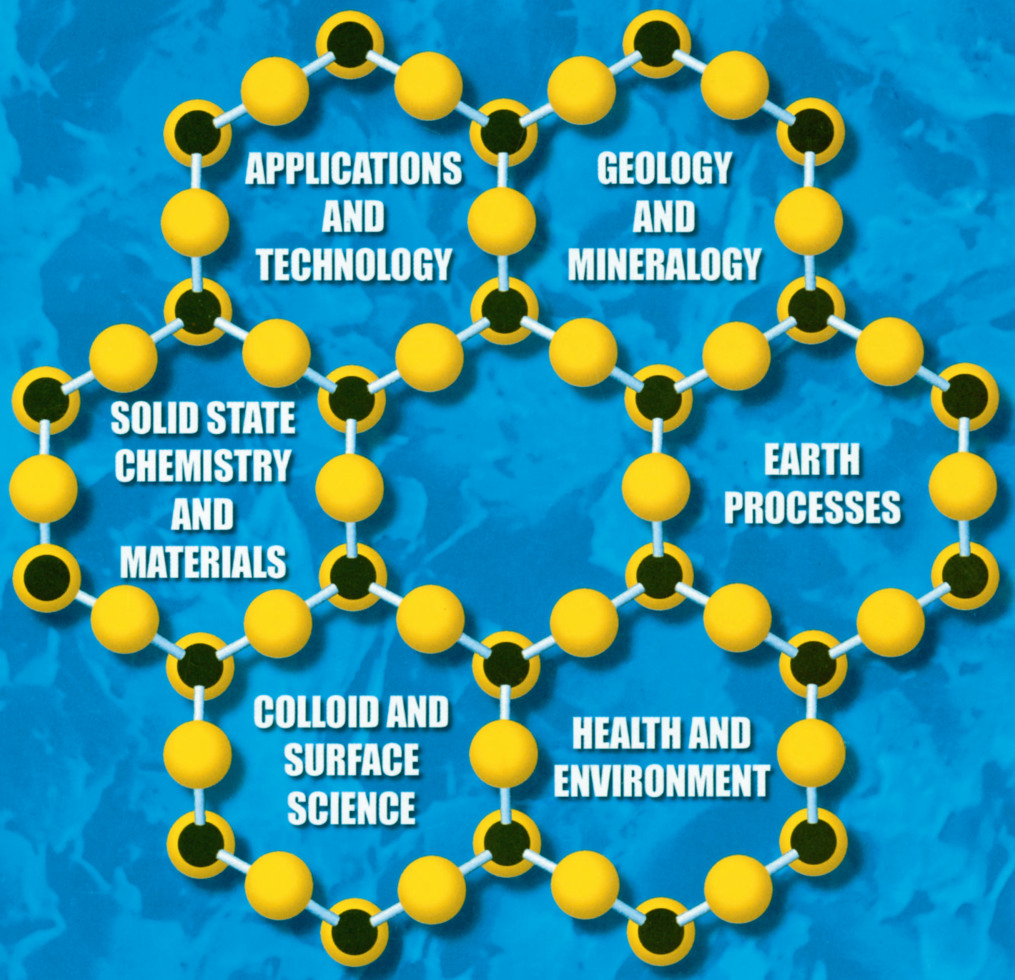

online at www.minersoc.org

Published by The Mineralogical Society

12 Baylis Mews, Amyand Park Road, Twickenham TW1 3HQ, UK

CLAY MINERALS

Journal of Fine Particle Science

VOLUME 51, NUMBER 3, June 2016

CONTENTS

ISSN 0009-8558

Typeset by Nova Techset Private Limited, Bengaluru and Chennai, India
Printed by Henry Ling Ltd., Dorchester, Dorset, UK

Clay Minerals, (2016) **51**, 457–467

Polysaccharide-halloysite nanotube composites for biomedical applications: a review

MINGXIAN LIU*, RUI HE, JING YANG, ZHERU LONG, BIAO HUANG, YONGWANG LIU AND CHANGREN ZHOU*

Department of Materials Science and Engineering, Jinan University, Guangzhou 510632, China

(*Received 8 November 2015; revised 14 December 2015; Guest Editor: Pooria Pasbakhsh*)

ABSTRACT: As a unique tubular nanoclay, halloysite nanotubes (HNTs) have recently attracted significant research attention. The HNTs have outer diameters of ~50 nm, inner lumens of ~20 nm and are 200–1000 nm long. They are biocompatible nanomaterials and widely available in nature, which makes them good candidates for application in biomedicine. Compared with other types of nanoparticles such as polymer nanoparticles and carbon nanotubes, the drawbacks associated with HNTs include brittleness, difficulty with fabrication, low fracture strength, high density and inadequate biocompatibility. Preparation of polysaccharide-HNT composites offer a means to overcome these shortcomings. Halloysite nanotubes can be incorporated easily into polysaccharides *via* solution mixing, such as with chitosan (CS), sodium alginate, cellulose, pectin and amylose, for forming composite films, porous scaffolds or hydrogels. The interfacial interactions, such as electrostatic attraction and hydrogen bonding, between HNTs and the polysaccharides are critical for improvement of the properties. Morphology results show that HNTs are dispersed uniformly in the composites. The mechanical strength and Young's modulus of the composites in both the dry and wet states are enhanced by HNTs and the HNTs can also increase the storage modulus, glass-transition temperature and thermal stability of the composites. Cytocompatibility results demonstrate that the polysaccharide-HNT composites have low cytotoxicity even for HNT loading >80%. Therefore, the polysaccharide-HNT composites show great potential for biomedical applications, *e.g.* as tissue engineering scaffold materials, wound-dressing materials, drug-delivery carriers, and cell-isolation surfaces.

KEYWORDS: halloysite, chitosan, alginate, interfacial interactions, cytocompatibility, mechanical properties.

Halloysite nanotubes (HNTs) have good mechanical properties, large aspect ratios, good biocompatibility, high porosity and are cheap (Joussein *et al.*, 2005; Liu *et al.*, 2014a). They offer potential for application in the improved tracking of cells, sensing of microenvironments, delivery of transfection agents, and scaffolding for incorporating in the host's body (Lvov *et al.*, 2013, 2015). In addition to significantly enhanced mechanical strength and good biocompatibility, HNTs have good hemostatic properties and wound-healing ability as reported by Qi *et al.* (2010) Liu *et al.* (2012b, 2013a, 2014b) and Zhai *et al.* (2013). The structure of HNTs is shown in Fig. 1A.

The drawbacks of HNTs for biomedical applications include brittleness, difficulty with fabrication, low fracture strength, high density, and inadequate biocompatibility (Lvov *et al.*, 2002; Levis & Deasy, 2003; Sun *et al.*, 2010). Polymer-HNT composites provide an alternative choice for overcoming these shortcomings of HNTs. Firstly, HNTs can be incorporated into polymer scaffolds providing structural

*E-mail: liumx@jnu.edu.cn (M.L.) and tcrz9@jnu.edu.cn (C.Z.)
DOI: 10.1180/claymin.2016.051.3.02

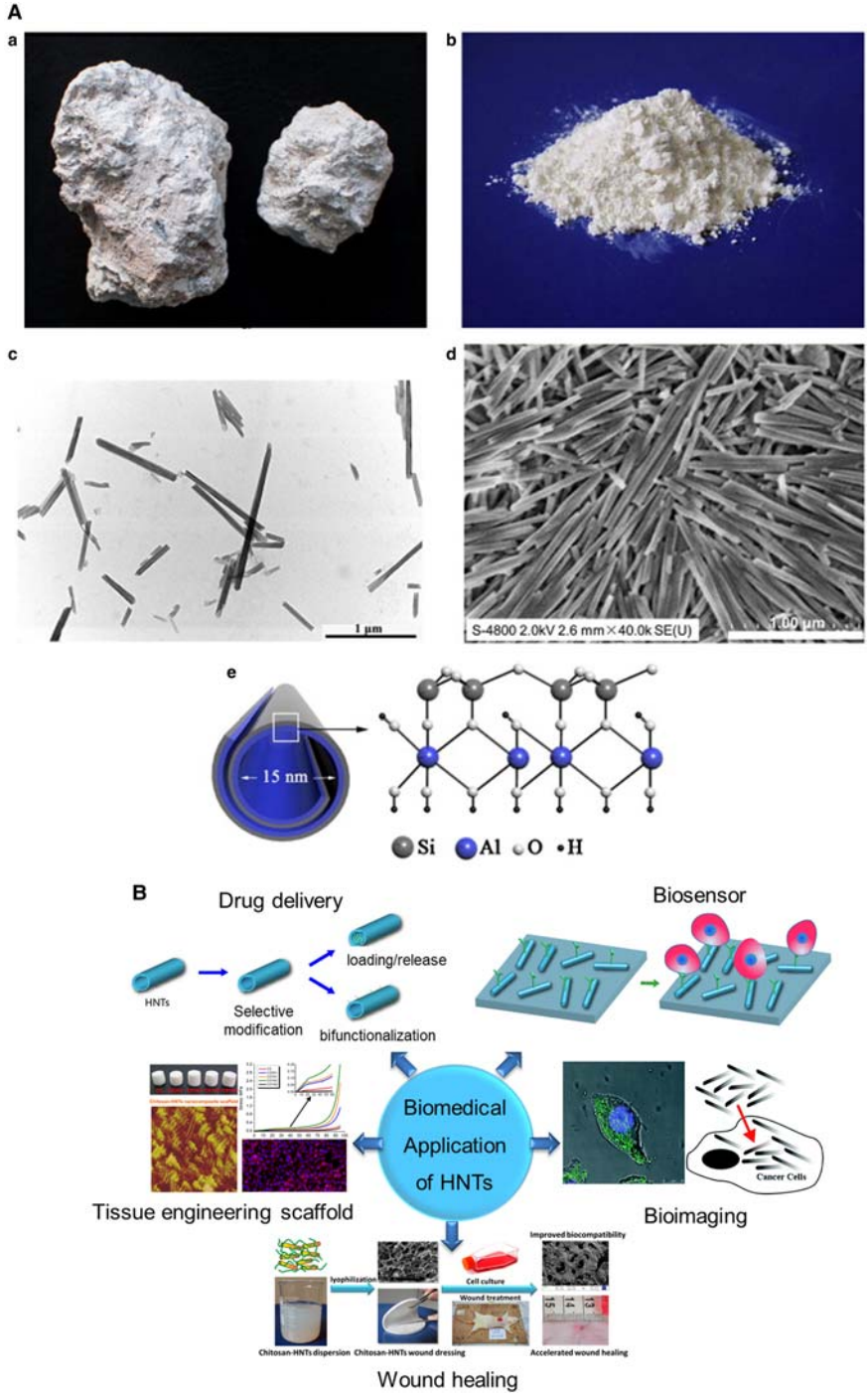

FIG. 1. The structure (A) and biomedical application (B) of HNTs. Part a is reproduced from Liu *et al.* (2014a) with the permission of Elsevier Science Ltd., Oxford, UK; part b is reproduced from Hughes & King (2010 and Liu *et al.*, 2013a, 2014) with the permission of The Royal Society of Chemistry and American Chemical Society, Washington DC, USA).

reinforcement as well as imparting novel properties such as promoting cell growth (Liu *et al.*, 2014a). The incorporation of HNTs can also enhance the blood clotting, platelet-activation ability, and wound-healing ability of chitosan (CS) (Liu *et al.*, 2014b). Bio-functionalization of HNTs has made it possible to generate a new class of bioactive nanocarriers which are conjugated with drugs, proteins, carbohydrates or nucleic acids for controlled delivery (Yah *et al.*, 2012). The HNT coatings on a microscale flow system can promote capture of leukemic and epithelial cancer cells from flow (Hughes & King, 2010; Mitchell *et al.*, 2015). The present research aims to translate these biotechnology-modified nanotubes into potential diagnostic and therapeutic applications. Figure 1B illustrates the biomedical applications of HNT-related materials.

Coating or mixing nanoparticles with a hydrophilic polymer shell can decrease significantly the toxicity and provide colloidal stability during blood circulation. Among the commercially available polymers, polysaccharides such as CS and sodium alginate, are very useful reagents in biology because of minimal toxicity, biocompatibility, protein resistance, good solubility in water and biodegradability. Due to the hydrophilicity of HNTs and their small dimensions, HNTs can be dispersed readily in water by mechanical stirring or ultrasonic treatment. As a result, they can be solution-mixed with polysaccharides in aqueous solutions for preparing composites (Sun *et al.*, 2010; Liu *et al.*, 2012b, 2013a, 2015; Zhai *et al.*, 2013). More importantly, the hydrogen bonding and electrostatic interactions between HNTs and polymers provide interfacial binding which assist with dispersion of the nanotubes. Unlike carbon nanotubes (CNTs), HNTs are abundant. Exploring the interactions between HNTs and CS is necessary because of the low cost and superior performance for biomedical applications. Previous study has shown that CS or polyethyleneimine (PEI)-coated HNTs had an additional delayed-release effect for drugs compared with raw HNTs (Lvov *et al.*, 2002; Levis & Deasy, 2003).

In the present study, we have summarized recent research progress in the biomedical application of polysaccharide-HNT composites. The interfacial interactions, preparation methods, structure and properties of the composites are discussed in detail. The cell viability assay and cell morphological observations were also investigated to demonstrate the influence of HNTs on the biocompatibility of polymers. Due to their performance and biocompatibility, the polysaccharide-HNT composites prepared have potential applications in tissue engineering, wound healing, biosensors and drug carrier systems. The critical issues and scientific challenges that require further research and development with respect to HNT composites in terms of practical biomedical applications are also discussed.

INTERFACIAL INTERACTIONS BETWEEN HNTS AND POLYSACCHARIDES

Due to the good water-dispersion ability of HNTs, polysaccharide-HNT composites are generally prepared *via* solution mixing. The HNTs can interact with the polysaccharides *via* electrostatic and hydrogen-bonding interactions when they are mixed. The interactions in the composites are of benefit for the formation of uniform dispersed composites and the improved properties.

Electrostatic interactions

Chitosan or sodium alginate can be dissolved in diluted aqueous solutions. Due to the protonation of the amines at low pH (<6), CS is positively charged in the solution. On the other side, HNTs are negatively charged on their outer surfaces due to isomorphous substitution of Al^{3+} for Si^{4+} (Tarì *et al.*, 1999). Therefore, when mixing CS with HNTs in solution at CS/HNTs ratios of 1:0.5 to 1:4, electrostatic attractions occur between them. Zeta potential measurements were used to investigate the electrostatic interactions between HNTs and CS. As expected, the surface charge of the HNTs in the aqueous dispersion is only slightly positive at very low pH values. As the pH value increased from 2 to 12, the surface charge fell sharply to reach a negative value. However, the CS-HNT hybrid showed a positive potential over the pH range of ~3–9. For example, the zeta potential value of a CS-HNT hybrid at pH 5.2 is 50.0 mV. This suggests that the positively charged CS can wrap the tubes *via* the electrostatic attractions. The CS-HNT hybrid becomes negatively charged when the pH is >9. This is due to fact that the amines in CS become deprotonated and the polymer loses its charge and becomes insoluble. The CS will precipitate gradually from the systems. Therefore, the zeta-potential of the CS-HNT hybrid is close to that of HNTs at higher pH values.

Hydrogen bonding interactions

The amine groups and hydroxyl groups on the polysaccharides can interact with the Si–O bonds or

Al-OH groups of HNTs *via* hydrogen bonding interactions (Liu *et al.*, 2012b, 2013a). Fourier transform infrared (FTIR) spectra were used to characterize the interactions between CS and HNTs in the composites. The two characteristic bands of CS at 1545 cm^{-1} and 1405 cm^{-1}, which correspond to the deformation vibrations of the protonated amine group ($-NH^{3+}$) and hydroxyl groups, respectively, shift to higher frequencies (*i.e.* the absorbance band of the NH_2 vibration moves from 1545 to 1548 cm^{-1} for the composites with 10% HNTs) due to the electrostatic interactions and hydrogen-bonding interaction between HNTs and CS. The broad bands around 3208 cm^{-1}, which are attributed to the overlapped N-H band and O-H band vibrations of CS, also move to higher frequencies in the composites. Therefore, FTIR results confirm the interactions between HNTs and CS *via* electrostatic interactions and hydrogen bonding.

Interfacial morphology of the polysaccharide-HNT hybrid

The surfaces of HNTs can be warped by polysaccharide chains due to the two types of interactions illustrated above. Atomic force microscopy (AFM) and transmission electron microscopy (TEM) were used to characterize the interfacial morphology of the polysaccharide-HNT hybrid (Liu *et al.*, 2013a, 2015). Raw HNTs exhibit cylindrical and open-ended tubular morphology. The walls of the tubes are clean. However, the walls of HNTs in the CS-HNTs or alginate-HNTs become rough and indistinct. From TEM images of polysaccharide-HNTs, an organic layer with light grey colour, which is ~20 nm thick, is located on the outer surfaces of HNTs. This phenomenon was also found in the amylose-HNT hybrid systems (Chang *et al.*, 2011). Both AFM and TEM results provide evidence for the presence of polysaccharides on HNT surfaces. Chitosan and alginate have good interfacial compatibility with HNTs.

PREPARATION AND STRUCTURE OF POLYSACCHARIDE-HNT COMPOSITES

Polysaccharide-HNT composites can be prepared by mixing the polymer and HNTs in aqueous solutions or in ionic liquid at room temperature. By drying the solutions under room temperature, thin composites films were obtained. For example, regenerated cellulose/HNT nanocomposite films with enhanced thermal and mechanical properties were prepared in ionic liquid (1-butyl-3-methylimidazolium chloride) using a solution casting method (Soheilmoghaddam & Wahit, 2013; Soheilmoghaddam *et al.*, 2013). In order to obtain the porous scaffolds, the solutions were frozen into ice at −20°C overnight in a refrigerator and then lyophilized at −80°C using a freeze drier. The dropwise addition of the polysaccharide-HNT solution into a precipitation bath containing NaOH or Ca^{2+} solution under mild stirring gave rise to composite hydrogel beads. On the other hand, glycerol-plasticized starch/HNT nanocomposites with improved tensile mechanical properties can also be prepared *via* melt-compounding (Schmitt *et al.*, 2012). Different materials exhibit different microstructures and HNT dispersion states.

Appearance of the polysaccharide-HNT composites

Due to the nanoscale dimension of the HNTs and the good dispersion in the polysaccharides matrix, the composite films are almost completely transparent and HNTs scarcely affect the light transmittance of the film even when the loading of HNTs is as high as 10% (Fig. 2) (Liu *et al.*, 2012b; Soheilmoghaddam & Wahit, 2013). Ultraviolet-visible (UV/vis) spectra of CS-HNT composite films show that all the composite films are >80% transparent across the visible-light spectrum (400–1000 nm). The change in transmittance of CS composite films with different HNT contents is <6%. The transmission of the cellulose-HNT nanocomposite films was reduced slightly even though they were kept above 85%, indicating perfect miscibility and compatibility (Soheilmoghaddam & Wahit, 2013). This is attributed to the fact that nano-scaled HNTs can be dispersed uniformly in the polysaccharides matrix which originated from the interfacial interactions between HNTs and polymer matrix.

The dispersion of the CS-HNT mixture was freeze-dried into self-supported sponge-like 3D porous scaffolds. The scaffolds retained the cylindrical shape of the mould in which they were freeze-dried without shape shrinkage being observed (Fig. 2) (Liu *et al.*, 2013a, 2014b). The shape and appearance of CS-HNT composite scaffolds were almost independent of the sample composition, indicating that HNTs have no effect on the formation of porous scaffolds. Alginate-HNT composite porous scaffolds also show a similar phenomenon (Liu *et al.*, 2015). All the scaffolds have a uniform shape in the form of a sponge. The HNTs have little influence on the colour, shape or porosity of the alginate scaffolds. An obvious stiffening of the

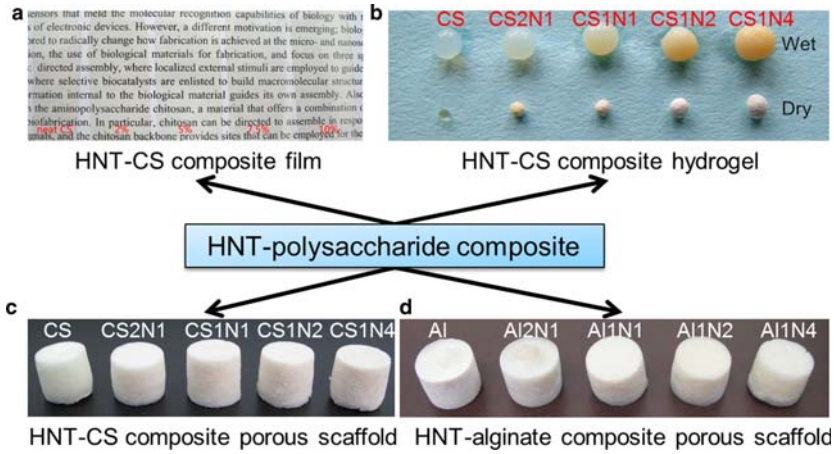

FIG. 2. Polysaccharide-HNT composites: the sample codes of the composite scaffold (CS2N1, CS1N1, CS1N2, CS1N4; Al, Al2N1, Al1N1, Al1N2, Al1N4) represent the weight ratio of CS (CS) or alginate (Al) and HNTs (N). (Figures 2a and 2b are reproduced from Liu *et al.* (2012b) and Peng *et al.* (2015), respectively, and are reproduced here with the permission of Elsevier Science Ltd., Oxford, UK.

composite scaffolds is found compared with the mechanically weak pure polysaccharide scaffolds according to the mechanical testing results.

The CS-HNT composite hydrogels were prepared by drop-wise addition of the dispersion of a CS-HNT mixture into a precipitation bath containing NaOH solution (Peng *et al.*, 2015). The appearance of the wet hydrogel bead and dry bead is shown in Fig. 2. The pure CS hydrogel bead was clear and transparent with a slight yellow colour. After incorporation of HNTs, the composite beads showed an opaque colour. This is due to the different dimensional distribution of the HNTs in the composite hydrogel.

Morphology of the polysaccharide-HNT composites

Due to the strong interfacial interactions, the dispersion state of HNTs in the polysaccharides matrix was satisfactory. The SEM images show that HNTs were dispersed uniformly in the CS composite film matrix and the interface between the HNTs and CS matrix was blurred (Fig. 3). An homogeneous distribution of the nanotubes into the low methoxyl pectin matrix was also found (Cavallaro *et al.*, 2013). As a result, the composite films showed a significantly improved mechanical and thermal performance compared with pure polymer film. When the loading of HNTs increased above 7.5%, the composites showed the morphology for a coexistence of both individually dispersed nanotubes and HNT aggregates, which is attributed to the re-aggregation of HNTs during the drying process of the films (Liu *et al.*, 2007).

The CS-HNT composite scaffolds were fabricated using a freeze-drying technique. Both pure CS and CS-HNT composite scaffolds exhibited a highly porous, open and 3D interconnected morphology with a pore size of ~200 μm (Liu *et al.*, 2013a). Addition of HNTs to CS had no significant influence on the microstructure for the scaffolds. The interactions between CS and HNTs can improve the stiffness and modulus of the porous scaffold. The increase in mechanical strength caused by the HNTs leads to a more homogeneous porous structure and less collapse of the pore walls. Meanwhile, the composite scaffolds had slightly larger pore sizes compared with that of a pure CS scaffold. As observed in high-magnification SEM images, the HNTs were exposed at the surfaces of the pores in the composite scaffolds. The exposed HNTs in the pore wall lead to enhancement of the roughness of the pore surface, which facilitates cell attachment and proliferation by acting as an anchor framework. The high-strength CS-HNT composite scaffolds prepared have potential applications in tissue engineering and wound healing due to their microstructures and their propensity for cell attachment and growth.

For the CS-HNT composite hydrogel beads, the outer surface of the beads is rough, while the inside of the beads contains a large number of HNTs (Peng *et al.*, 2015). The HNTs were disordered and coated

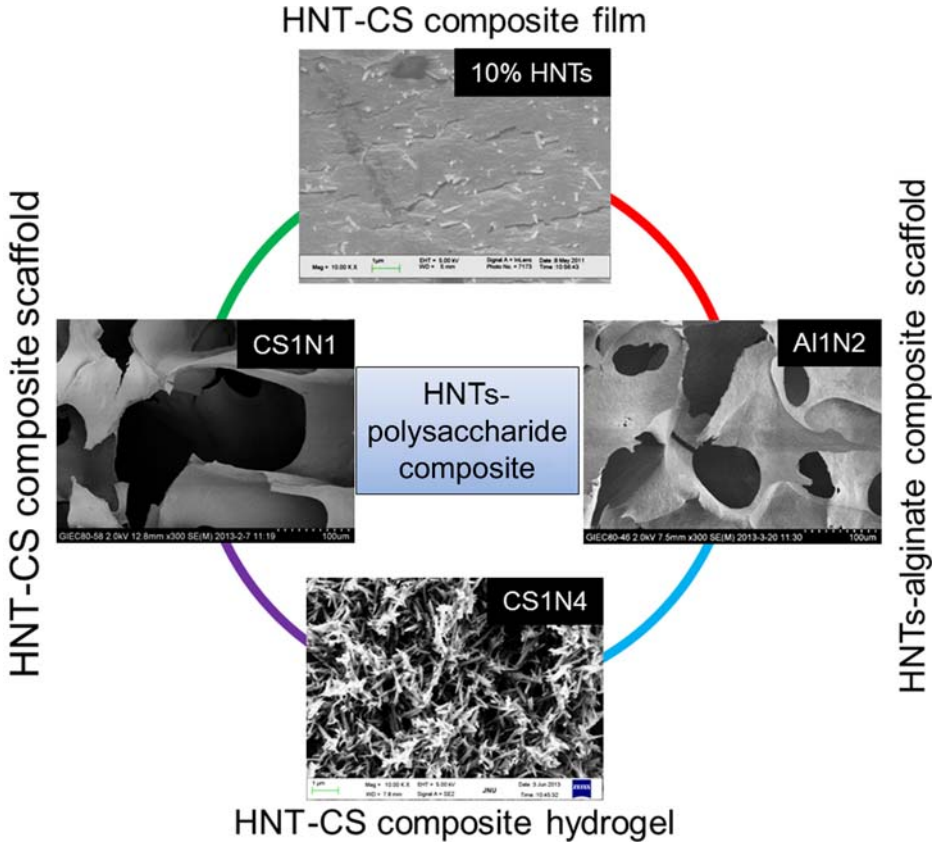

FIG. 3. Morphologies of the polysaccharide-HNT composites.

with CS, indicating that HNTs are immobilized completely by the CS inside. The nanotubes also appeared at the peel of the composite beads. When investigating the core structure of the dried hydrogel beads, the HNTs were more numerous there than at the peel. This can be understood by the fact that the formation of the hydrogel beads is attributed to the pH-precipitation of CS solution. In contrast, pure CS bead exhibited a smooth outer and inner surface, indicating a uniform structure.

Crystal structure of the polysaccharide-HNT composite

The crystal structures of polysaccharide-HNT composites can be investigated by X-ray diffraction (XRD). For pure CS scaffolds, a broad scattering reflection is located at ~20°2θ, indicating that it is amorphous in the present preparation condition (Liu *et al.*, 2013a). The HNTs exhibit diffraction peaks at 12°2θ, 20°2θ and 25°2θ which are assigned to the (001), (02, 11) and (020) planes of HNTs, respectively (Brindley *et al.*, 1946). The locations of the diffraction peaks of HNTs in the composite remained unchanged, indicating that no intercalation of CS into the interlayer of tube walls occurred. The intensity of the (001) reflection relative to the (02,11) band increased with increase in HNT loading, indicating that a partial orientation of HNTs took place in the composite (Liu *et al.*, 2013b).

Microcrystalline cellulose/1-allyl-3-methylimidazolium chloride/HNT dispersions displayed stronger birefringence with increasing HNTs content, and became intensely birefringent when sheared (Luo *et al.*, 2014). The composite fibres were then prepared from the mixture dispersions with liquid crystal (LC) phases by a wet-spinning method. The thermal stability, tensile strength and moisture-barrier properties of the cellulose nanocomposite fibres were found to have improved significantly compared with those of the pure fibre.

PROPERTIES OF POLYSACCHARIDE-HNT COMPOSITES

Mechanical properties of the polysaccharide-HNT composites

Due to rigid silicate nanotubes with large aspect ratios and interfacial reactions taking place between HNTs and the polysaccharide matrix, the polysaccharide-HNT composites exhibit significantly improved mechanical properties such as tensile properties, compressive properties, and dynamic mechanical properties both in the dry and wet states.

The HNT can effectively improve both tensile strength and Young's modulus of CS composite films up to 7.5% HNT loading (Liu *et al.*, 2012b; De Silva *et al.*, 2013). The tensile strength and tensile modulus for CS-HNT composites with 7.5% HNTs were 54.2 and 1240 MPa, which are 134% and 65% greater than those of the pure CS, respectively. The addition of HNTs into cellulose also increased the tensile strength of the nanocomposite films up to a loading of 6 wt.%. The cellulose/HNT composite containing 6 wt.% HNTs exhibited a remarkable 55.3% increase in tensile strength (Soheilmoghaddam *et al.*, 2013). Polyethylene glycol (PEG)-modified HNTs can be distributed well in a starch matrix and thus the tensile strength of the composite films was clearly enhanced. However, the elongation at break of the composite film decreased compared with the pure CS film. The modulus of the composite films increased with increase in HNT content until a loading of 7.5% HNTs suggesting the reinforcing effect of HNTs on CS. The decreased strength and Young's modulus of composites with larger HNT contents (>7.5%) are related to the presence of HNT aggregates in the composites. In another report (De Silva *et al.*, 2013), the CS-HNT composite membranes with 5 w/w% of HNTs were found to have the highest Young's modulus and tensile strength, showing a 21% and a 34% increase in the Young's modulus and tensile strength, respectively, compared with pure CS membrane. The CS-HNT composite films also show greater storage modulus values in the glassy and the rubbery states. For example, the storage modulus of the composite film with 7.5% HNTs at 100°C and 200°C is 193% and 119% greater than those of pure CS, respectively.

The CS-HNT composite scaffolds also exhibited improved compressive mechanical performance (Liu *et al.*, 2013a). Pure CS scaffold is soft, spongy and elastic, and the compressive strength is ~0.16 MPa. By incorporating HNTs, the stress of the composite scaffold was significantly greater than that of pure CS throughout the tested strain range. The increasing trend of stress is also proportional to the HNT loading. The stress at 80% strain for CS1N4 (weight ratio of CS and HNTs is 1:4) was 0.55 MPa, which is ~17 times greater than that of a pure CS scaffold. The compression modulus of composite scaffolds is also significantly greater than that of pure CS. The maximum compression modulus of the composite scaffold was 450.6 kPa with 80 wt.% HNT which is greater than that of previously reported CS/HA composite scaffolds (Thein-Han & Misra, 2009) and the data is comparable with those of CS/CNTs composite scaffolds (Sweetman *et al.*, 2008). Incorporation of HNTs into CS can increase the density of the scaffold due to the larger amount of material in the CS-HNT dispersion. Also, HNTs can interact with CS *via* electrostatic attraction and hydrogen bonding as illustrated before, which leads to the improved Young's modulus of CS (Liu *et al.*, 2012b). Alginate-HNT composite scaffolds are also stronger and more robust than pure alginate scaffold (Liu *et al.*, 2015). The stress at the same strain of the composite scaffolds is far greater than that of the pure alginate scaffolds. From the initial stage of the stress-stain curves, the slope of the composite scaffolds is greater than that for the pure alginate sample. This suggests that the increased compressive modulus of the composite scaffolds is comparable to that of the pure alginate scaffold.

It is important to determine the mechanical properties of the tissue engineering porous scaffolds in the wet state because the scaffolds need to contact the body fluids when they are implanted in the body. The compressive properties of the alginate-HNT composite scaffolds in the wet state were tested after soaking the scaffolds in PBS solution for 24 h. The elastic modulus, the stress at 40% strain, and the stress at 60% strain of the alginate scaffold increased significantly after incorporation of the HNTs. For example, elastic modulus of the alginate-HNTs (weight ratio of alginate and HNTs is 1:2) composite, the stress at 40% strain, and the stress at 60% strain were 25.4, 8.0, and 13.8 kPa, respectively, which is 3.0, 3.6, and 2.4 times greater than those of the pure alginate scaffold, respectively. Therefore, the alginate-HNT composite scaffolds can tolerate much greater loadings in both the dry and the wet states.

Thermal properties of the polysaccharide-HNT composites

The glass-transition temperature (T_g) and thermal stability of polysaccharides can also be affected by the

addition of HNTs. The T_g value of the CS-HNT composites increased consistently with increase in HNT loading (Liu *et al.*, 2012b). The maximum T_g of the composites was 172°C for the composites with 10% HNTs, which was 12°C higher than that of pure CS. In addition, the intensity of the loss tangent (tan δ) peaks for composites is less than that of pure CS, as the CS can dissipate more energy applied to the sample due to its viscous response at high temperature.

The interactions between HNTs and CS can also affect the thermal stability of the CS-HNT composites (Liu *et al.*, 2013a; Peng *et al.*, 2015). The degradation temperature of CS is increased slightly by the addition of HNTs, while the degradation temperature of HNTs is decreased slightly compared to pristine HNTs. For example, for the CS1N4 sample (weight ratio of CS and HNTs = 1:4), the degradation temperatures of CS and HNT components were 277 and 477°C, which are 4°C higher and 6°C lower than pure CS and pristine HNTs, respectively. De Silva *et al.* (2013) also found that the corresponding temperatures of CS-HNT membranes at 50% remaining weight had increased drastically compared with pure CS. The increase in the thermal stability of CS is attributed to the effective delay in mass transport during the thermal decomposition *via* the addition of HNTs.

Adsorption and release properties of the polysaccharide-HNT composites

The effects of HNTs on the adsorption behaviour of CS hydrogel beads were investigated using methylene blue (MB) and malachite green or ammonium in aqueous solution (Zheng & Wang, 2009; Peng *et al.*, 2015).

Zheng & Wang (2009) prepared CS-HNT composite hydrogel and used it as the adsorbent to remove ammonium from synthetic wastewater. The composite showed comparable adsorption capacity to that of pure polymer hydrogel for NH_4^+ removal. The adsorption equilibrium was achieved within 5 min with an equilibrium adsorption capacity of 27.7 mg N/g and monolayer adsorption capacity of 40.9 mg N/g (30 wt. % HNTs). The adsorption process was pH-independent within pH 4.0–7.0, and the adsorption capacity of the composite hydrogel was not affected over the cycles of adsorption studied (five cycles). Glutaraldehyde cross-linked CS-HNTs composite shows excellent capacity for horseradish peroxidase (HRP) immobilization (Zhai *et al.*, 2013). The CS-HNT composites prepared with the immobilized HRP exhibited a high overall removal efficiency for phenol from wastewater.

Peng *et al.* (2015) also prepared the CS-HNTs composite hydrogel for removal of MB and malachite green dyes. The equilibrium adsorption amounts of CS, CS1N1 (weight ratio of CS and HNTs is 1:1), CS1N4 (weight ratio of CS and HNTs is 1:4) hydrogel beads were 67.49, 68.92, and 72.60 mg g^{-1}, respectively towards MB, indicating an increased absorption ability through the incorporation of HNTs. The numerous active sites (hydroxyl groups) on HNTs are related to the fast rates of adsorption in the initial adsorption period. With active sites gradually occupied by the adsorbed dyes, the adsorption rates decrease gradually. When the active sites are fully occupied, the amount adsorbed cannot increase any more even by extending the adsorption time, and the adsorption equilibrium is reached at this point. The adsorption kinetics of MB by the composite hydrogel bead can be described well by the pseudo-second-order model which implies that the overall rate of the adsorption process was controlled by chemisorption.

Then alginate-HNT composite hydrogel beads were prepared by dropping the solution of mixture into 2% (m/V) calcium chloride solution by syringe under continuous stirring (Liu *et al.*, 2012a). The removal of MB dye from aqueous solution by the alginate-HNT composite hydrogel beads was assessed. Compared with the pure alginate beads, not only was the adsorption capacity of alginate-HNT hybrid beads improved but the stability in the solution was also enhanced significantly. The pH value and temperature had small effects on the adsorption capacity of alginate–HNT composite beads. The maximum adsorption capacity was ~222 mg/g at 298 K and 250.00 mg/g at 308 K for the alginate-HNT composite (1/1, w/w) hydrogel bead. More importantly, after ten successive adsorption–desorption cycles, the removal efficiency of MB could be kept at >90%. Column research indicated that the removal efficiency could be maintained above 90% after 1500 bed volumes of waste water were treated. Cavallaro *et al.* (2013) also found that alginate-HNT composite hydrogel beads showed an improved ability to capture crystal violet dye (Cavallaro *et al.*, 2013). Therefore, alginate-HNT hybrid beads have important implications in the enhancement of controlled adsorptions.

Sodium alginate/hydroxyapatite (HA)/HNT composite hydrogel beads can also be used to adsorb and release the diclofenac sodium drug (DS) (Fan *et al.*, 2013). It was found that the weight ratio of HNTs to alginate and the concentration of alginate influenced the entrapment efficiency (EE) and release of DS. The EE was enhanced from 62.85% ± 0.29% to 74.63% ± 1.65%, and the undesirable burst release of

DS was overcome by introducing appropriate amounts of HA and HNTs. The release rate of DS from the composite beads was 9.19 mg g^{-1} h^{-1}. The release of DS is controlled by Case-II transport. The tubular structure of the HNTs and the HA nanoparticles formed *in situ* affect the improved drug loading and release behaviour of the drug, because the nanoparticles can restrict the mobility of the alginate chains.

A novel anticancer drug-delivery system based on HNTs loaded with triazole dye brilliant green (BG) and coated with dextrin (DX) were designed by Dzamukova *et al.* (2015). The DX stoppers reduced the release of BG by half compared with uncoated tubes, allowing for enhanced drug delivery by means of the open tubes. This platform also benefited from the effective uptake of the biocompatible HNTs by lung carcinoma cells (A549), followed by the hydrolysis of the DX coating with cellular glycosyl hydrolases, facilitating the release of the drug from the nanotubes and the subsequent inhibition of mitochondria in the cells. Electrospun poly(caprolactone)/gelatin microfibre membranes embedded with drug-loaded HNTs were also found to extend release of the drugs to a period of 20 days, compared to 4 days when admixed directly into the microfibres (Xue *et al.*, 2015).

Biocompatibility of the polysaccharide-HNT composites

The increased use of HNTs in a variety of biomedical applications will require stringent toxicological assessment *in vitro* and *in vivo*. Although a limited number of studies have looked into the toxicity profile of HNTs (Vergaro *et al.*, 2010; Fakhrullina *et al.*, 2015), we offer here a summary regarding the cytotoxic profile of polysaccharide-HNT composites.

The cytotoxicity of polysaccharide-HNT composites was assessed using fibroblasts and endothelial cells. The results reveal that 3T3 cells can adhere and proliferate on both pure CS and CS-HNT composites (Liu *et al.*, 2012b, 2013a) (Fig. 4). With increasing culturing time, the absorbance for all the samples increased, indicating the growth of the cells. No visible reduction in viability between the CS and CS-HNT composites were found at 1, 3 and 7 days of culturing time, which suggests that the CS-HNT composites have good cytocompatibility. The cells grown on both CS and CS-HNT composite films were shown to be well expanded in typical spindle morphologies and formed tight intercellular junctions with adjacent cells. Slight differences in cell morphology are found among the cells grown on pure CS film and on the composite

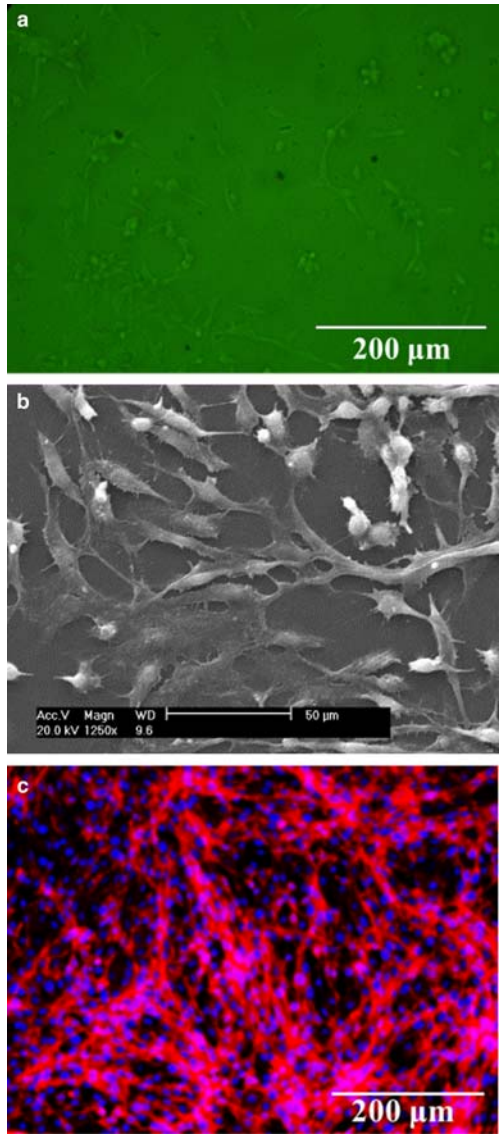

FIG. 4. NIH-3T3 cell morphology on the CS-HNT composites with 10 wt.% HNTs loading: (a) optical image taken using an Olympus CXK41 inverted microscope; (b) SEM image; (c) fluorescent micrographs.

films. Interestingly, the cell surfaces tend to be flatter on CS-HNT composites compared with pure CS. This may be attributed to the much greater roughness of the composite surfaces. In a high-magnification SEM image, the cells are seen to be anchored to substrate surfaces by discrete filopodia exhibiting numerous microvilli. The increased surface roughness and the presence of Si in the composite surface are beneficial to the attachment of the

cells. Hence, HNTs had little influence on the cytocompatibility of CS. The CS-HNT composites prepared can be used as a cell-culture scaffold.

The *in vivo* biocompatibility of the CS-HNT composites were studied in a wound-repair experiment. It was found that the wound-healing ability of CS porous sponges was increased by HNTs (Liu *et al.*, 2014b). The regenerated skin treated with the CS-HNT composite sponges was smooth and similar to normal skin without scar formation after 4 weeks, indicating the good healing ability for skin tissue. The CS-HNT composite sponges had much greater wound-healing rates and contraction ability than those of pure CS sponges. The composite sponges showed 3.4–21-fold increased closure ratios compared with the pure CS after 1 week of treatment. In particular, the CS1N4 sponges showed the greatest closure ratio of 22%. After 2 weeks, the wounds treated with the CS-HNT composite sponges exhibited linearly increased closure ratios with the increase in the HNT loading. For example, the wound closure of CS1N4 sponges is ~85%, which is 32% greater than that of pure CS sponges. The maximum wound closure at day 28 was 98.0%, which corresponds to the CS1N1 group. This value is notably larger than that of pure CS groups, at only 87%. In conclusion, the CS-HNT composites show improved wound-healing ability and can be used as wound-dressing materials.

BIOMEDICAL APPLICATIONS OF POLYSACCHARIDE-HNT COMPOSITES

Due to the simple preparation process, improved mechanical and thermal properties, and good biocompatibility of polysaccharide-HNT composites, they have great potential as biomedical materials. The field of application includes tissue engineering, wound healing, biosensors and drug-carrier systems. For example, the CS-HNT or alginate-HNT composites can be used as tissue engineering for supporting cell growth. The polysaccharide-HNT composite hydrogels can be used as drug delivery carriers or wound healing materials. The polysaccharide-grafted HNTs have also shown controlled-release ability for drugs and improved blood- and cyto-compatibility.

However, major gaps in basic knowledge remain, with the major obstacles confronting the HNT field being the lack of a detailed understanding of the effect of nanotube dimensions on biocompatiblity. How to separate the tubes by their diameter and length is unknown. It is also highly desirable to achieve surface patterns of HNTs with well controlled spatial arrangements for cell-growth supporting materials. In addition, a method of assessing the distribution and biodegradation behaviour of HNTs *in vivo* needs to be devised. Based on these research advances, we believe that the nanotechnology-derived products of HNTs can assist in the treatment and diagnosis of disease.

ACKNOWLEDGEMENTS

This work was supported financially by the National High Technology Research and Development Program of China (2015AA020915), the National Natural Science Foundation of China (grant No. 51473069 and 51502113), the Guangdong Natural Science Funds for Distinguished Young Scholars (grant No. S2013050014606), and the Fundamental Research Funds for the Central Universities (21615204).

REFERENCES

Brindley G., Robinson K. & MacEwan D. (1946) The clay minerals halloysite and meta-halloysite. *Nature*, **157**, 225–226.

Cavallaro G., Gianguzza A., Lazzara G., Milioto S. & Piazzese D. (2013) Alginate gel beads filled with halloysite nanotubes. *Applied Clay Science*, **72**, 132–137.

Chang P.R., Xie Y., Wu D. & Ma X. (2011) Amylose wrapped halloysite nanotubes. *Carbohydrate Polymers*, **84**, 1426–1429.

De Silva R., Pasbakhsh P., Goh K.-L., Chai S.-P. & Ismail H. (2013) Physico-chemical characterisation of chitosan/halloysite composite membranes. *Polymer Testing*, **32**, 265–271.

Dzamukova M.R., Naumenko E.A., Lvov Y.M. & Fakhrullin R.F. (2015) Enzyme-activated intracellular drug delivery with tubule clay nanoformulation. *Scientific Reports*, **5**.

Fakhrullina G.I., Akhatova F.S., Lvov Y.M. & Fakhrullin R.F. (2015) Toxicity of halloysite clay nanotubes in vivo: A caenorhabditis elegans study. *Environmental Science: Nano*, **2**, 54–59.

Fan L., Zhang J. & Wang A. (2013) In situ generation of sodium alginate/hydroxyapatite/halloysite nanotubes nanocomposite hydrogel beads as drug-controlled release matrices. *Journal of Materials Chemistry B*, **1**, 6261–6270.

Hughes A.D. & King MR. (2010) Use of naturally occurring halloysite nanotubes for enhanced capture of flowing cells. *Langmuir*, **26**, 12155–12164.

Joussein E., Petit S., Churchman J., Theng B., Righi D. & Delvaux B. (2005) Halloysite clay minerals – a review. *Clay Minerals*, **40**, 383–426.

Levis S. & Deasy P. (2003) Use of coated microtubular halloysite for the sustained release of diltiazem hydrochloride and propranolol hydrochloride. *International Journal of Pharmaceutics*, **253**, 145–157.

Liu M., Guo B., Du M. & Jia D. (2007) Drying induced aggregation of halloysite nanotubes in polyvinyl alcohol/halloysite nanotubes solution and its effect on properties of composite film. *Applied Physics A*, **88**, 391–395.

Liu L., Wan Y., Xie Y., Zhai R., Zhang B. & Liu J. (2012a) The removal of dye from aqueous solution using alginate-halloysite nanotube beads. *Chemical Engineering Journal*, **187**, 210–216.

Liu M., Zhang Y., Wu C., Xiong S. & Zhou C. (2012b) Chitosan/halloysite nanotubes bionanocomposites: Structure, mechanical properties and biocompatibility. *International Journal of Biological Macromolecules*, **51**, 566–575.

Liu M., Wu C., Jiao Y., Xiong S. & Zhou C. (2013a) Chitosan–halloysite nanotubes nanocomposite scaffolds for tissue engineering. *Journal of Materials Chemistry B*, **1**, 2078–2089.

Liu M., Zhang Y. & Zhou C. (2013b) Nanocomposites of halloysite and polylactide. *Applied Clay Science*, **75**, 52–59.

Liu M., Jia Z., Jia D. & Zhou C. (2014a) Recent advance in research on halloysite nanotubes-polymer nanocomposite. *Progress in Polymer Science*, **39**, 1498–1525.

Liu M., Shen Y., Ao P., Dai L., Liu Z. & Zhou C. (2014b) The improvement of hemostatic and wound healing property of chitosan by halloysite nanotubes. *RSC Advances*, **4**, 23540–23553.

Liu M., Dai L., Shi H., Xiong S. & Zhou C. (2015) In vitro evaluation of alginate/halloysite nanotube composite scaffolds for tissue engineering. *Materials Science and Engineering: C*, **49**, 700–712.

Luo Z., Wang A., Wang C., Qin W., Zhao N., Song H. & Gao J. (2014) Liquid crystalline phase behavior and fiber spinning of cellulose/ionic liquid/halloysite nanotubes dispersions. *Journal of Materials Chemistry A*, **2**, 7327–7336.

Lvov Y., Price R., Gaber B. & Ichinose I. (2002) Thin film nanofabrication via layer-by-layer adsorption of tubule halloysite, spherical silica, proteins and polycations. *Colloids and Surfaces A: Physicochemical and Engineering Aspects*, **198**, 375–382.

Lvov Y. & Abdullayev E. (2013) Functional polymer-clay nanotube composites with sustained release of chemical agents. *Progress in Polymer Science*, **38**, 1690–1719.

Lvov Y., Wang W., Zhang L. & Fakhrullin R. (2016) Halloysite clay nanotubes for loading and sustained release of functional compounds. *Advanced Materials*, **28**, 1227–1250.

Mitchell M.J., Castellanos C.A. & King M.R. (2015) Surfactant functionalization induces robust, differential adhesion of tumor cells and blood cells to charged nanotube-coated biomaterials under flow. *Biomaterials*, **56**, 179–186.

Peng Q., Liu M., Zheng J. & Zhou C. (2015) Adsorption of dyes in aqueous solutions by chitosan–halloysite nanotubes composite hydrogel beads. *Microporous and Mesoporous Materials*, **201**, 190–201.

Qi R., Guo R., Shen M., Cao X., Zhang L., Xu J., Yu J. & Shi X. (2010) Electrospun poly(lactic-co-glycolic acid)/halloysite nanotube composite nanofibers for drug encapsulation and sustained release. *Journal of Materials Chemistry*, **20**, 10622–10629.

Schmitt H., Prashantha K., Soulestin J., Lacrampe M. & Krawczak P. (2012) Preparation and properties of novel melt-blended halloysite nanotubes/wheat starch nanocomposites. *Carbohydrate Polymers*, **89**, 920–927.

Soheilmoghaddam M. & Wahit M.U. (2013) Development of regenerated cellulose/halloysite nanotube bionanocomposite films with ionic liquid. *International Journal of Biological Macromolecules*, **58**, 133–139.

Soheilmoghaddam M., Wahit M.U., Mahmoudian S. & Hanid N.A. (2013) Regenerated cellulose/halloysite nanotube nanocomposite films prepared with an ionic liquid. *Materials Chemistry and Physics*, **141**, 936–943.

Sun X., Zhang Y., Shen H. & Jia N. (2010) Direct electrochemistry and electrocatalysis of horseradish peroxidase based on halloysite nanotubes/chitosan nanocomposite film. *Electrochimica Acta*, **56**, 700–705.

Sweetman L.J., Moulton S.E. & Wallace G.G. (2008) Characterisation of porous freeze dried conducting carbon nanotube-chitosan scaffolds. *Journal of Materials Chemistry*, **18**, 5417–5422.

Tarì G., Bobos I., Gomes C.S. & Ferreira J.M. (1999) Modification of surface charge properties during kaolinite to halloysite-7 transformation. *Journal of Colloid and Interface Science*, **210**, 360–366.

Thein-Han W.W. & Misra R.D.K. (2009) Biomimetic chitosan-nanohydroxyapatite composite scaffolds for bone tissue engineering. *Acta Biomaterialia*, **5**, 1182–1197.

Vergaro V., Abdullayev E., Lvov Y.M., Zeitoun A., Cingolani R., Rinaldi R. & Leporatti S. (2010) Cytocompatibility and uptake of halloysite clay nanotubes. *Biomacromolecules*, **11**, 820–826.

Xue J., Niu Y., Gong M., Shi R., Chen D., Zhang L. & Lvov Y. (2015) Electrospun microfiber membranes embedded with drug-loaded clay nanotubes for sustained antimicrobial protection. *ACS Nano*, **9**, 1600–1612.

Yah W.O., Takahara A. & Lvov Y.M. (2012) Selective modification of halloysite lumen with octadecylphosphonic acid: New inorganic tubular micelle. *Journal of the American Chemical Society*, **134**, 1853–1859.

Zhai R., Zhang B., Wan Y., Li C., Wang J. & Liu J. (2013) Chitosan–halloysite hybrid-nanotubes: Horseradish peroxidase immobilization and applications in phenol removal. *Chemical Engineering Journal*, **214**, 304–309.

Zheng Y. & Wang A. (2009) Enhanced adsorption of ammonium using hydrogel composites based on chitosan and halloysite. *Journal of Macromolecular Science, Part A*, **47**, 33–38.